RESEARCH ARTICLE | OCTOBER 05 2023

Universal scaling of shear thickening transitions

Meera Ramaswamy ; Itay Griniasty ; Danilo B. Liarte ; Abhishek Shetty ; Eleni Katifori ; Emanuela Del Gado ; James P. Sethna ; Bulbul Chakraborty ; Itai Cohen

J. Rheol. 67, 1189–1197 (2023)
https://doi.org/10.1122/8.0000697

Universal scaling of shear thickening transitions

Meera Ramaswamy,[1,a)] Itay Griniasty,[1] Danilo B. Liarte,[1] Abhishek Shetty,[2] Eleni Katifori,[3] Emanuela Del Gado,[4] James P. Sethna,[1] Bulbul Chakraborty,[5] and Itai Cohen[1]

[1]*Department of Physics, Cornell University, Ithaca, New York 14853*
[2]*Anton Paar USA, 10215 Timber Ridge Drive, Ashland, Virginia 23005*
[3]*Department of Physics, University of Pennsylvania, Philadelphia, Pennsylvania 19104*
[4]*Department of Physics, Georgetown University, Washington DC 20057*
[5]*Department of Physics, Brandeis University, Waltham, Massachusetts 02454*

(Received 21 May 2023; final revision received 8 September 2023; published 5 October 2023)

Abstract

Nearly, all dense suspensions undergo dramatic and abrupt thickening transitions in their flow behavior when sheared at high stresses. Such transitions occur when the dominant interactions between the suspended particles shift from hydrodynamic to frictional. Here, we interpret abrupt shear thickening as a precursor to a rigidity transition and give a complete theory of the viscosity in terms of a universal crossover scaling function from the frictionless jamming point to a rigidity transition associated with friction, anisotropy, and shear. Strikingly, we find experimentally that for two different systems—cornstarch in glycerol and silica spheres in glycerol—the viscosity can be collapsed onto a single universal curve over a wide range of stresses and volume fractions. The collapse reveals two separate scaling regimes due to a crossover between frictionless isotropic jamming and frictional shear jamming, with different critical exponents. The material-specific behavior due to the microscale particle interactions is incorporated into a scaling variable governing the proximity to shear jamming, that depends on both stress and volume fraction. This reformulation opens the door to importing the vast theoretical machinery developed to understand equilibrium critical phenomena to elucidate fundamental physical aspects of the shear thickening transition. © *2023 The Society of Rheology.*
https://doi.org/10.1122/8.0000697

I. INTRODUCTION

Suspensions of solid particles in a liquid commonly exhibit shear thickening, an increase in the shear viscosity with the applied stress or strain rate [1,2]. This increase in viscosity can span orders of magnitude and even lead to solidification, as illustrated by people running atop vats of cornstarch [3].[1] Such strong shear thickening behavior has been attributed to the change in the nature of particle interactions—at low stresses, the particle interactions are dominated by the lubrication forces, but at high stresses, the particle surfaces are forced closer together and frictional contact interactions dominate [3–9].

Understanding the mechanism underpinning the thickening transition has led to numerous studies focused on altering the system properties to modify the shear thickening behavior. Commonly, two different strategies have been pursued —(1) changing the interparticle friction and (2) changing the particle microstructure or suspension packing. Changes to the interparticle friction can be achieved by altering the particle surface roughness [7,10–15], interparticle adhesion [16], or hydrogen bonding [17–19]. The maximum particle packing in the suspensions can be altered by tuning the particle shape [20–22], size or polydispersity [23,24], or applying external fields [25–31]. In many of these examples, even a small change in the suspension can result in large changes to the rheology. It has, therefore, been a major challenge to develop a unified, suspension-independent framework to predict shear thickening.

A major step toward developing such a framework was proposed by Wyart and Cates [5,6], who modeled the viscosity as a function of the distance to a stress-dependent jamming volume fraction. As the stress increases, the contacts between the particles become frictional and the jamming volume fraction decreases, resulting in an increase in the viscosity. This theory has been used to fit experimental and simulation data with varying degrees of success [22,23,32–34]. Others have proposed similar models to describe shear thickening [29,32,35], and more recently, the extent of shear thickening has also been shown to be related to the jamming volume fraction [36], indicating that jamming underpins the shear thickening transition. Intriguingly, it has been shown that equilibrium statistical mechanics can be used to study the quasistatic nonequilibrium jamming transition [37–41]. Despite these close connections between shear thickening and jamming, however, the relationship between the shear thickening and statistical scaling frameworks remains unexplored. More specifically, it is yet unclear if shear thickening can be described by the proximity to the jamming critical point via universal scaling functions and if jamming with and without shear are associated with the same universality class and scaling exponents.

In this work, we adopt the idea of scaling to analyze the experimentally observed viscosity of two different shear

a)Author to whom correspondence should be addressed; electronic mail: mr944@cornell.edu
[1]Search www.youtube.com for walking on cornstarch

thickening suspensions and establish the relationship between shear thickening and the associated critical points. Since the advent of the ideas of universality and scaling in equilibrium phase transitions [42], it has been known that scaling analysis provides a litmus test for the presence of critical points in complex phase diagrams. This approach led to the discovery of nonclassical exponents associated with phase transitions, the identification of universality classes, and the development of the renormalization group [42]. In contrast to fitting data to functional forms, scaling involves collapsing data over a broad range of multiple control parameters. The advantage of this approach is that it is model-independent and often reveals the underlying physical governing principles, the relevant variables controlling the distance to critical points, and the associated scaling functions. Here, we propose to use the same machinery to investigate the critical points associated with the shear thickening transition.

More specifically, we pursue the idea that the rheology of shear thickening suspensions is governed by two different critical points and that a *crossover scaling framework* can be utilized to characterize this transition [42]. Crossover scaling was originally introduced to describe transitions between thermodynamic critical points (e.g., Heisenberg magnets with small uniaxial anisotropy behaving like Ising models) and has become invaluable for describing finite-temperature behavior induced by quantum critical points [43–45], crossovers between universality classes in random matrix theory [46], and fracture and depinning transitions [47]. Our analysis shows that the same framework provides an excellent unified description of thickening transitions.

II. RECASTING THE WYART AND CATES MODEL

We begin by recasting the Wyart and Cates [5] model, the current state-of-the-art model used to describe shear thickening, into the framework of crossover scaling. Briefly, the model expresses the viscosity of the suspension in terms of a distance to a stress-dependent jamming volume fraction, $\phi_J(\sigma)$,

$$\eta \sim (\phi_J(\sigma) - \phi)^{-2}. \tag{1}$$

As the stress increases, the nature of the contact forces between the particles in the suspension changes from hydrodynamic to frictional and the jamming volume fraction decreases as

$$\phi_J(\sigma) = \phi_0(1 - f(\sigma)) + \phi_\mu f(\sigma). \tag{2}$$

Here, $f(\sigma)$ is the fraction of frictional contacts in the system, ϕ_0 is the jamming volume fraction in the absence of friction, and ϕ_μ is the jamming volume fraction when all the interactions between the particles are frictional ($\phi_\mu < \phi_0$). $f(\sigma)$ is a sigmoidal function of the applied stress, with limits of zero at low stress and one at high stress, and Eq. (2) defines a line of critical points at which the viscosity diverges, leading to shear-induced jamming at finite σ. Thus, increasing the stress activates frictional contacts, which lowers the jamming volume fraction and increases the viscosity. Despite its simplicity, this model does a remarkable job capturing essential features of the flow behaviors including continuous shear thickening, discontinuous shear thickening, and shear jamming.

To recast this model into the crossover scaling framework, we substitute Eq. (2) into Eq. (1) to obtain

$$\eta \sim (\phi_0(1 - f(\sigma)) + \phi_\mu f(\sigma) - \phi)^{-2}. \tag{3}$$

Pulling out a factor of $(\phi_0 - \phi)^{-2}$, we find that the viscosity can be expressed as a function that only depends on a specific combination of $f(\sigma)$ and $\phi_0 - \phi$,

$$\eta(\phi_0 - \phi)^2 \sim \mathcal{F}_{WC}\left(\frac{f(\sigma)}{\phi_0 - \phi}\right), \tag{4}$$

where the crossover scaling function $\mathcal{F}_{WC}$, specific to the Wyart and Cates model is

$$\mathcal{F}_{WC} \sim \left(\frac{1}{\phi_0 - \phi_\mu} - \frac{f(\sigma)}{\phi_0 - \phi}\right)^{-2}. \tag{5}$$

At small values of the scaling variable, $x_{WC} = f(\sigma)/(\phi_0 - \phi)$, the scaling function is a constant and the system behavior is governed by the frictionless jamming critical point $\eta \sim (\phi_0 - \phi)^{-2}$ at zero shear. Crucially, however, the crossover scaling function $\mathcal{F}_{WC}$ has a divergence at $x_c = 1/(\phi_0 - \phi_\mu)$ indicating that as $x_{WC}/x_c \to 1$, the system is governed by a line of frictional jamming critical points such that $\eta \sim (x_c - x_{WC})^{-2}$. Notably, with this form of the crossover scaling function, the viscosity diverges with exactly the same exponent of -2 all along the jamming line. This recasting of the Wyart and Cates model for the thickening transition in terms of crossover scaling clearly indicates that a major assumption in the model is that frictionless and frictional shear jamming (at nonzero x_{WC}) are controlled by the same fixed point and that the only effect of friction is to change the location of the critical point.

Practically, this formulation enables us to move beyond merely fitting the model to viscosity data and, instead, attempt a scaling collapse to elucidate the underlying physics controlling this transition. More specifically, Eq. (4) suggests that plotting $\eta(\phi_0 - \phi)^2$ as a function of $f(\sigma)/(\phi_0 - \phi)$ should collapse the viscosity across various stresses and volume fractions onto a universal curve, revealing the scaling function and its singularities. This collapse will also allow us to determine whether thickening is indeed controlled by a unique scaling exponent.

III. EXPERIMENTAL METHODS

We test this scaling theory on two different noninertial, low Reynolds number systems—a mixture of cornstarch in glycerol and a mixture of hard sphere silica particles in glycerol both of which show shear thickening behavior but over different ranges of volume fractions. The samples were prepared by weighing out the solutes, cornstarch (Argo) and silica (2 μm charge stabilized spheres from Angstrom Sphere), and the solvent, glycerol (Sigma-Aldrich). We use

glycerol as the solvent in each of these cases because of its low vapor pressure and the ease with which these glycerol-based suspensions can be loaded onto the rheometer. The cornstarch suspensions were used immediately after preparation and the silica suspensions were sonicated for 60 min prior to use. The viscosity of the suspension is measured using a stress-controlled method on an Anton Paar MCR 702 Rheometer. We use a 50 mm stainless steel parallel plate geometry at a set gap of 1 mm. To prevent slip at higher volume fractions and stresses, we used sanded plates. The sample was presheared at a constant stress of 1 Pa for 5 min. The suspension viscosity was then measured by performing a descending stress ramp.

The viscosity of the cornstarch and silica suspensions of different volume fractions as a function of the stress are shown in Figs. 1(a) and 1(b), respectively. The low volume fraction data [yellow and light pink data in Figs. 1(a) and 1(b), respectively] have smaller viscosities and mild shear thickening or continuous shear thickening (CST). The intermediate volume fraction data [teal and purple data in Figs. 1(a) and 1(b), respectively] have larger viscosities and show discontinuous shear thickening (DST), where $d\log(\eta)/d\log(\sigma) \geq 1$.

IV. RESULTS

To collapse the viscosity using Eq. (5), we need to determine the isotropic jamming fraction at zero shear, ϕ_0, and the fraction of frictional contacts, $f(\sigma)$. We determine ϕ_0 from the divergence of the low stress viscosity (see the supplementary material for details [78]). We use the form $f(\sigma) = e^{-\sigma^*/\sigma}$ for the fraction of frictional contacts, which is consistent with fits of the Wyart and Cates model in prior literature [34,48]. We have explored a limited set of different expressions for $f(\sigma)$, none of which qualitatively change the results reported here [see the supplementary material for results with a different functional form of $F(\sigma)$ [78]]. By fitting the flow curves in Figs. 1(a) and 1(b) to the Wyart

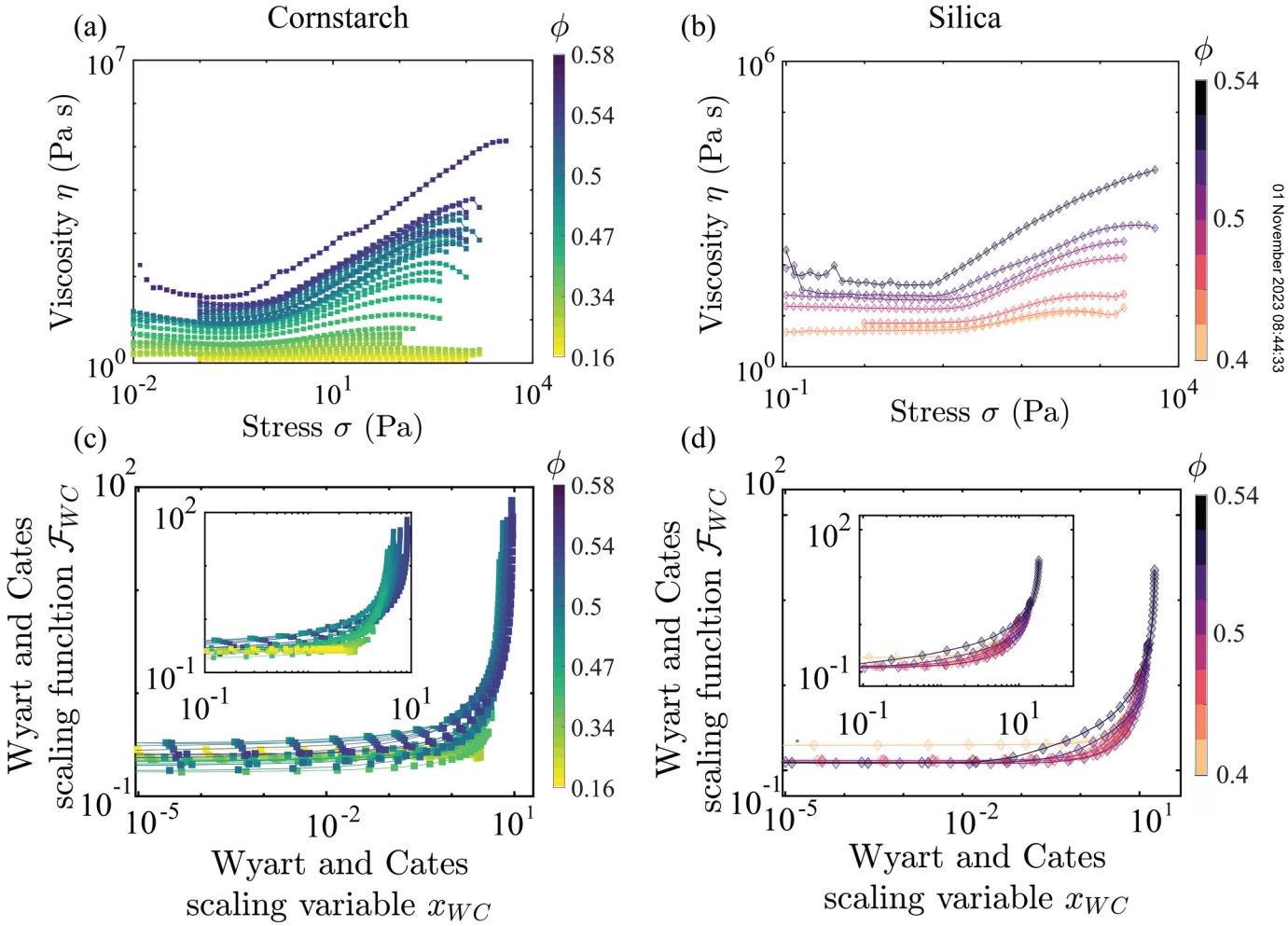

FIG. 1. Viscosity versus stress measurements and scaling predictions from the Wyart and Cates model. (a) and (b) The viscosity as a function of applied stress for (a) cornstarch suspensions with volume fractions ranging from 0.16 (yellow) to 0.54 (dark blue) and (b) silica suspensions with volume fractions ranging from 0.4 (light pink) to 0.52 (black). These suspensions show a range of shear thickening behavior across volume fractions from weakly shear thickening to discontinuous shear thickening to shear jamming. The solid lines are linking data points for added ease of visualization. (c) and (d) Plots of the predicted Wyart and Cates scaling function $\mathcal{F}_{WC} = \eta(\phi_0 - \phi)^2$ versus the Wyart and Cates scaling variable $x_{WC} = f(\sigma)/(\phi_0 - \phi)$ for cornstarch suspensions (c) and silica suspensions (d), showing promising but incomplete scaling collapse. The inset shows the zoom-in of the high x_{WC} region. In the inset of (c), the cornstarch scaling function diverges at ~10 at low volume fractions, ~6 at intermediate volume fractions, and ~ 10 at large volume fractions. The silica data in the inset of (d) diverges at ~10 at low volume fractions and ~20 at large volume fractions.

and Cates model, we determine σ^*. Using the calculated values of $f(\sigma)$, and ϕ_0, we plot $\mathcal{F}_{WC} = \eta(\phi_0 - \phi)^2$ as a function of $x_{WC} = e^{-\sigma^*/\sigma}/(\phi_0 - \phi)$ in Figs. 1(c) and 1(d). While we find that the collapse is promising, at higher volume fractions, the data diverge at different values of x_{WC} (Fig. 1, insets). Since this reformulation of the Wyart and Cates model in the language of crossover scaling assumes a very particular form of the scaling function, $\mathcal{F}_{WC}$, and the scaling variable, x_{WC}, we naturally ask whether relaxing these assumptions and using the full machinery of crossover scaling leads to better data collapse and a more accurate description of the observed thickening transitions.

We find that using a scaling variable where the numerator is both a function of stress and volume fraction, $x = g(\sigma, \phi)/(\phi_0 - \phi)$ dramatically improves the scaling collapse (Fig. 2). To simplify the search for the function, $g(\sigma, \phi)$, we assume a product form, $g(\sigma, \phi) = C(\phi)f(\sigma)$. Impressively, this single parameter, $C(\phi)$, for the data set at each volume fraction collapses both the cornstarch and silica suspension data across all measured volume fractions onto a single universal scaling function $\mathcal{F}$ as shown in Fig. 2(a) [49]. Interestingly, these two suspensions represent a broad range of thickening materials in many ways—cornstarch is more dramatic, with a large discontinuous shear thickening regime, while the equivalent regime in the "model" silica suspension is much smaller. The fact that in each suspension, all of the viscosity versus stress curves collapse onto each other, and the fact that the curves from both suspensions collapse is a strong indication that this scaling function $\mathcal{F}$ is universal.

The scaling function has several characteristic features that are consistent with the expected behavior for shear thickening suspensions. At small x, $\mathcal{F}$ is a constant, and the divergence in the viscosity is

$$\eta \sim \frac{1}{(\phi_0 - \phi)^2}, \tag{6}$$

which is consistent with a number of previous studies

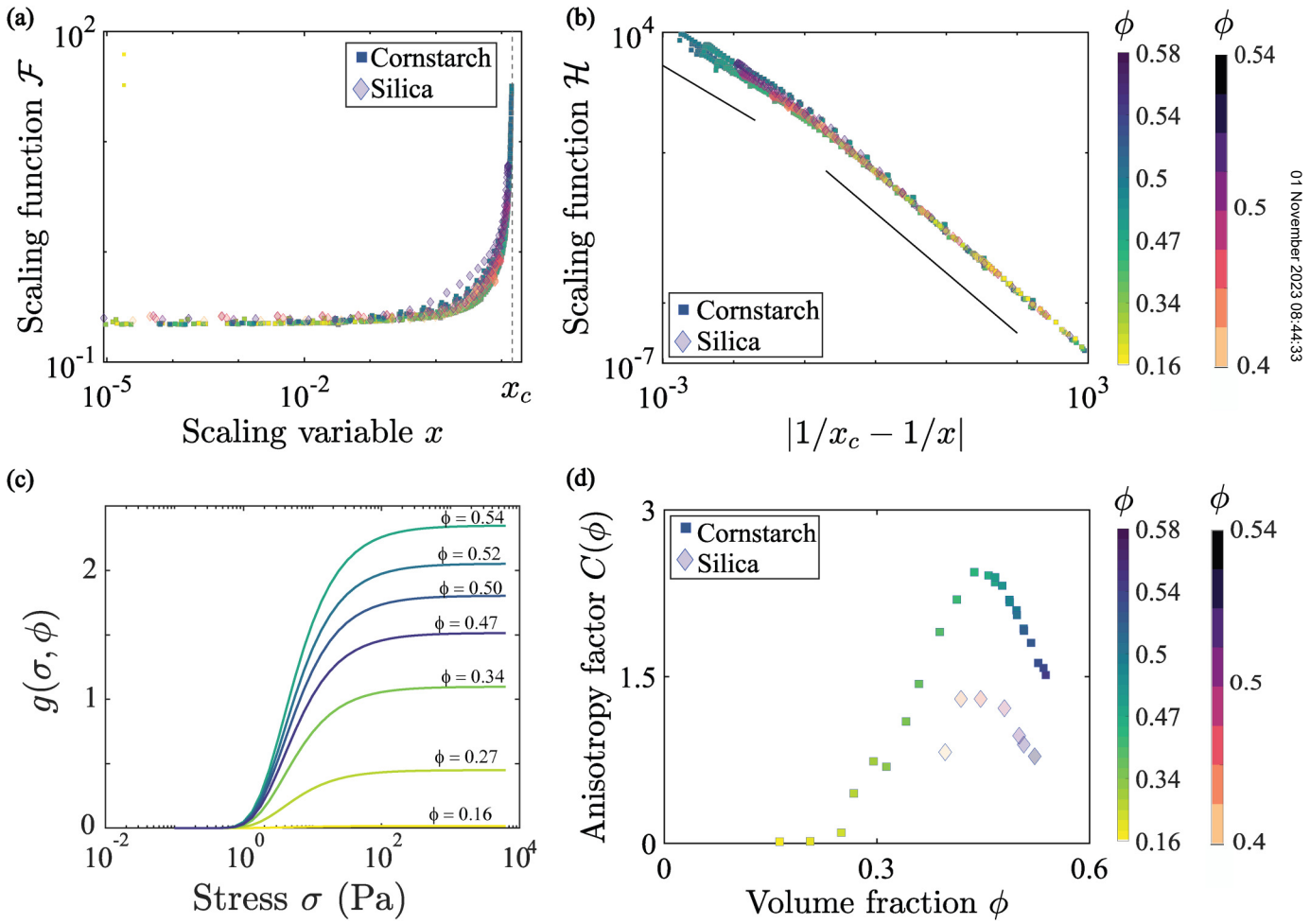

FIG. 2. Universal scaling of the suspension viscosity. (a) The scaling function $\mathcal{F} = \eta(\phi_0 - \phi)^2$ as a function of the scaling variable $x = e^{-\sigma^*/\sigma}C(\phi)/(\phi_0 - \phi)$ for all the cornstarch (squares) and silica (diamond) suspensions data. We find that all the data collapse onto a single universal curve that diverges at $x = x_c$. (b) The scaling function $\mathcal{H} = \eta g^2(\sigma, \phi)$ versus $|1/x_c - 1/x|$ for all the cornstarch and silica suspensions data. This way of scaling the data clearly illustrates two distinct regimes—a regime characterized by a power law of -2 at small x and a power law of $\sim -3/2$ at $x \approx x_c$. The solid black lines indicate power laws of -2 and -1.5, respectively. (c) The nonlinear scaling variable, $g(\sigma, \phi)$, as a function of the stress for a range of volume fractions of the cornstarch suspensions. We note that this parameter has the same sigmoidal shape, now well established for the fraction of frictional contacts, while $C(\phi)$ dramatically affects the overall scale. (d) The anisotropy factor $C(\phi)$ as a function of the volume fraction for both silica and cornstarch. We note that $C(\phi)$ is a smooth analytic function as required by theories for scaling variables such as $g(\sigma, \phi) = f(\sigma)C(\phi)$ far from the critical point.

[23,32,50,51]. As x increases, $\mathcal{F}$ also increases, until it diverges at $x = x_c$, with an exponent δ,

$$\mathcal{F}(x) \sim \frac{1}{(x_c - x)^{\delta}}, \tag{7}$$

with $x_c = 14.5$. We note that since $C(\phi)$ is a multiplicative factor, there is an overall scale that can be chosen for x_c.

This divergence implies that the viscosity also diverges with the exponent δ. Remarkably, we find that $\delta < 2$ and is significantly different from the exponent observed for frictionless isotropic jamming (see supplementary material, Fig. S3 [78]). To visualize this change in exponents, we follow Cardy [42, Sec. 4.2] and write

$$\eta g^2(\sigma, \phi) \sim \mathcal{H}(|1/x_c - 1/x|), \tag{8}$$

where $\mathcal{H}$ is a universal scaling function. We then plot $\eta g^2(\sigma, \phi)$ as a function of $|1/x_c - 1/x|$ in Fig. 2(b). We find excellent collapse over seven orders of magnitude in the scaling variable with two easily distinguishable regimes each characterized by clearly different power-law exponents. At small x, far from x_c, the behavior is governed by the frictionless jamming point ϕ_0 and $\mathcal{H} \sim |1/x_c - 1/x|^{-2}$. As x approaches x_c, we observe a clear change in the value of the exponent from -2, with a crossover between the two regimes at $x/x_c \sim 0.1$. Our best estimate for the new exponent is $-3/2$. Importantly, this change in exponent indicates that the crossover underlying shear thickening is between critical points that belong to *different* universality classes. As such, this change in exponent is a remarkable demonstration of frictional shear-jamming being qualitatively different from frictionless jamming at zero shear.

Importantly, the nonlinear scaling variable that drives the suspension toward frictional jamming, $g(\sigma, \phi)$, depends on both the stress and the volume fraction as shown in Fig. 2(c). $g(\sigma, \phi)$ is sigmoidal in the stress, similar to the fraction of frictional contacts, $f(\sigma)$, in previous works [5,23,33]. The volume fraction dependence changes the overall scale and indicates that the fraction of frictional contacts that contribute to and determine the shear viscosity varies with ϕ. The scaling collapse of the data reveals that this functional dependence, $C(\phi)$, is nonmonotonic for both the silica and cornstarch suspensions [Fig. 2(d)]. Once these material-dependent differences in $C(\phi)$ and ϕ_0 are accounted for, the collapse is universal.

Since the scaling form [Eq. (8)] is universal and valid at all stresses and volume fractions, we can use it to construct a shear thickening phase diagram as shown in Fig. 3 [52]. Crucially, constructing these phase diagrams is only possible because we have determined the full functional form of the scaling function over seven orders of magnitude in the scaling variable, which is not typical for other analyses. In particular, we plot the shear jamming boundary at $x = x_c$ (border of the red region) where the system transitions from a flowing to a jammed state. Since this border is defined by the scaling variable x_c, it is independent of the details of the scaling function $\mathcal{F}$ (shape, functional form, etc.). In addition, the boundary for discontinuous shear thickening is determined from

$$\frac{d\log(\eta)}{d\log\sigma} = 1, \tag{9}$$

which *does* depend on the form of the scaling function. To obtain this boundary (blue lines), we fit $\mathcal{H}$ to a function consisting of two power law regimes stitched together by a crossover region (see the supplementary material [78]) and use this fit to compute the derivatives in Eq. (9). This boundary indicates the transition from continuous to discontinuous shear thickening regimes. Due to the form of the anisotropy factor $C(\phi)$ and differences in ϕ_0 and σ^*, the phase diagrams for cornstarch and silica are distinct and are shown in Figs. 3(a) and 3(b), respectively. These phase diagrams are qualitatively

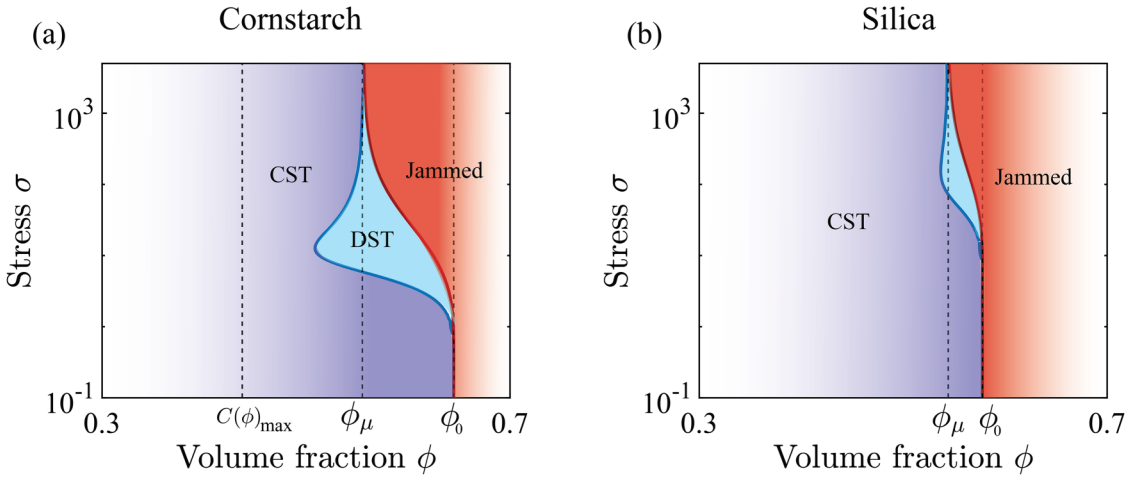

FIG. 3. Phase diagrams for cornstarch and silica suspensions as derived from the scaling analysis. Three distinct regions are seen in the phase diagrams for the cornstarch (a) and silica (b) systems—continuous shear thickening (CST) in purple (light gray), discontinuous shear thickening (DST) in blue (medium gray) and a jammed region in red (dark gray). The shear jamming line (maroon) demarcating the jammed and DST regions is determined by $x = x_c$, where $x = e^{-\sigma^*/\sigma} C(\phi)/(\phi_0 - \phi)$ and the DST line (blue) boundary between CST and DST regions is determined by the condition $d\log\eta/d\log\sigma = 1$. The vertical dotted lines indicate the values of the frictionless jamming point, ϕ_0, and shear jammed point, ϕ_μ, and the volume fraction at which $C(\phi)$ is maximum.

similar to those obtained by previous experiments and simulations [8,53,54] but are generated directly from the scaling collapse of the data.

V. DISCUSSION

A. Altering the scaling variable to change material properties

A key modification that enabled scaling collapse of the data is the nonlinear scaling variable, $g(\sigma, \phi) = f(\sigma)C(\phi)$, that depends on *both* the stress and the volume fraction. Previous studies have interpreted $f(\sigma)$ as the fraction of frictional contacts. If we retain this interpretation, then the inclusion of $C(\phi)$ in $g(\sigma, \phi)$ suggests that only a portion of $f(\sigma)$ contributes to the viscosity divergence. Such modulation of $f(\sigma)$ is indicative of the role of force network connectivity or anisotropy in the viscosity divergence consistent with recent simulations [29,55,56] and models [29,35,57]. More specifically, one hypothesis is that the function $C(\phi)$ is related to the anisotropy of the force network. We would expect the anisotropy to be low for both low and high volume fractions. At low volume fractions, the suspension is too sparse for contacts to build up, while at high volume fractions, chains along the maximal compression axis fuse into an isotropic network. The anisotropy is expected to be high at intermediate volume fractions. Recent simulation results [29,55,56] and proposed models that incorporate the system microstructure [29,35,57] support the inclusion of anisotropy as a parameter governing shear thickening. Another hypothesis is that $C(\phi)$ is a measure of the connectivity of the network and its contribution to the viscosity divergence. Initially, we expect the connectivity of the force network to increase with increasing volume fraction. However, at higher volume fractions, not all the particles in the force network contribute to the viscosity, leading to a decrease in $C(\phi)$. In this interpretation, we could further hypothesize that the peak in $C(\phi)$ could be correlated to the emergence of the first frictional rigid clusters of particles. This emergence has been shown to occur before the onset of DST (dilatant shear thickening) and at a constant volume fraction, consistent with the behavior of $C(\phi)$ measured here [58].

Interpreting $g(\sigma, \phi)$ in this manner enables us to envision how we can alter the shear thickening phase diagram. In particular, by modifying material properties corresponding to changes in σ^*, ϕ_0, and $C(\phi)$, we can dramatically shift the borders between the jammed and unjammed regimes and by extension the discontinuous versus continuous shear thickening. A change in σ^*, for example, indicates how easily frictional interactions increase with stress and can be controlled by altering particle roughness [7,10–15], hydrogen bonding [17–19], or solvent-particle interactions [59]. Changes to ϕ_0 can be generated by modifying particle roughness [10–15,60], shape [20–22], and polydispersity [23,24]. Finally, differences in $C(\phi)$ may result from the constraints governing particle displacements and rotations as well as other perturbations to the flows [25–28,36,56,61–63]. Thus, differences in these variables directly inform the types of changes that one can use to influence the thickening and jamming behaviors.

B. Exponents related to frictionless and frictional divergence

The scaling analysis in Fig. 2(b) illustrates two distinct power law regimes, one with an exponent of -2, associated with frictionless at zero shear (frictionless isotropic jamming) and the other with an exponent of $-3/2$ associated with frictional shear jamming. Measurements of the divergence in the viscosity associated with frictionless and frictional jamming have been reported previously in a wide range of systems. Our -2 scaling result for frictionless isotropic jamming is consistent with a number of previous studies in shear thickening suspensions [23,32,50,51].

We note that in pressure-driven suspensions there is a claim that the scaling exponent in this regime is -2.85. This apparent discrepancy, however, is a result of an assumption that stress and pressure scale identically close to jamming, which may not hold for dense suspensions. For the expert reader, previous works have shown a scaling of $(\phi_0 - \phi) \sim \mathcal{J}^{\gamma_\phi}$, with $\gamma_\phi = 0.37$ for frictionless particles and $\gamma_\phi = 0.7$ for frictional suspensions [64,65,75]. Here, $\mathcal{J} = \eta_0\dot{\gamma}/P$ is the viscous number, η_0 is the solvent viscosity, $\dot{\gamma}$ is the shear rate and P is the applied pressure [64–67]. Assuming that $P \sim \sigma$ close to jamming, we can invert the equation to obtain $\eta \sim (\phi_0 - \phi)^{-1/\gamma_\phi} = (\phi_0 - \phi)^{-2.85}$ in the frictionless regime, giving an apparent discrepancy in the scaling exponent [64]. The assumption that $P \sim \sigma$ however, is a conjecture and may not hold for dense suspensions. Indeed, a recent study extending the analysis presented here has shown that the pressure and the shear viscosities are associated with different scaling exponents [68,69]. In these simulations, the shear viscosity exponents are consistent with those presented here and the pressure viscosity exponents are consistent with those presented in the pressure-driven systems [68].

With respect to the exponent of $-3/2$ for the shear jamming regime, we note that others have previously tried to fit exponents to viscosity versus volume fraction data. Our result is well within the range of previously obtained exponents [23,32,48,70]. Moreover, here, we use scaling collapse of the entire shear thickening transition, using a scaling variable that is a function of stress and the volume fraction to determine both exponents. This approach is more rigorous since multiple measurements corresponding to different combinations of stress and volume fraction are used to determine the value of the universal function $\mathcal{F}$ at each point x.

C. Renormalization group flows

Recasting the nonequilibrium thickening transition as being governed by crossover scaling between two different critical points suggests a renormalization group flow diagram with two fixed points. This picture is directly analogous to that found in equilibrium magnetic systems (e.g., Heisenberg to Ising crossover scaling). We project the flows, obtained from the experimentally determined scaling function, onto the $g(\sigma, \phi)$ and $|\phi_0 - \phi|$ plane (Fig. 4). The nonlinear scaling variable, $g(\sigma, \phi) = f(\sigma)C(\phi)$, is associated with the relevant direction at the frictionless jamming point with the nonlinear terms in $g(\sigma, \phi)$ providing analytic corrections to

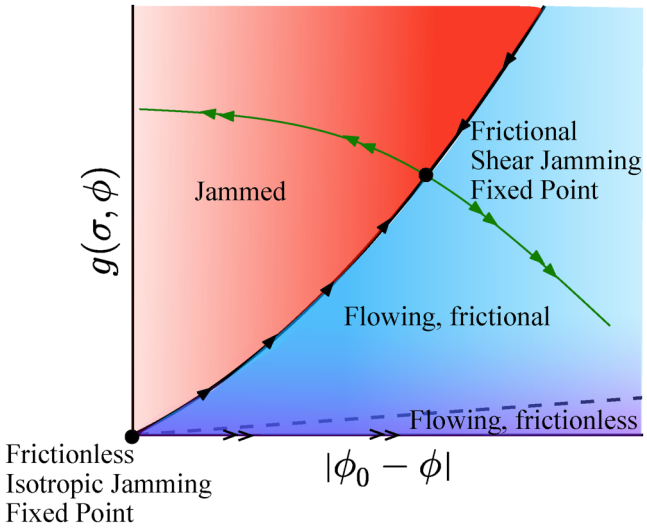

FIG. 4. Renormalization group flow diagram governing the shear thickening transition. We plot the projection of the renormalization group flows onto the $g(\sigma, \phi)$ and $|\phi_0 - \phi|$ plane. The two distinct fixed points are the frictionless isotropic jamming fixed point and the frictional shear jamming fixed point. The black solid line with single arrows is a line of critical points, and the dashed line corresponds to the x value for the knee in Fig. 2(b). The flows are outward from the isotropic jamming point, which corresponds to a critical exponent of -2 along the $|\phi_0 - \phi|$ axis. The green line (solid double arrows) is the outward flow line for the shear jammed fixed point, which corresponds to a critical exponent of $-3/2$ for the viscosity.

scaling [71]. The isotropic jamming fixed point has two relevant directions with flows away from the fixed point. The first is along the $|\phi_0 - \phi|$ axis (black line double arrows) and the second is along the line of critical points on the shear-jamming line (black line single arrow) flowing to the shear jamming fixed point. This critical manifold separates the jammed and the flowing states. The shear jamming fixed point must also have a relevant variable, and the flow along this line determines the exponent δ (drawn schematically in green line double arrows). Finally, the crossover between the two fixed points can be approximated by the knee in Fig. 2(b) and is depicted in the renormalization group flow by the dashed gray line. This diagram clearly illustrates the deep connection between the shear thickening transition and renormalization group flows that are the hallmark of critical phenomena in thermodynamic systems.

VI. CONCLUSIONS

Adopting this statistical mechanics framework to describe shear thickening opens several novel avenues for future work. For instance, universal scaling theories and scaling functions such as those presented have previously been used to predict a number of physical properties in equilibrium systems, suggesting that similar approaches may be used in shear thickening. In the well-studied system of Heisenberg and Ising magnets, for example, one can use the crossover scaling function to determine the specific heat, correlation functions, and many other system properties [42]. Similarly, recent studies have investigated the scaling relations for the jamming transition for frictionless particles, demonstrating that both static and dynamic viscoelastic properties such as the shear stress, bulk modulus, and shear modulus can be predicted by such a scaling formulation [37,38,40,41,72,73,76,77]. These studies demonstrate the power of scaling theories and universal scaling functions, and our work suggests that analogous predictions and theories could be generated for shear thickening and frictional jamming.

ACKNOWLEDGMENTS

The authors thank Edward Y. X. Ong, Eric M. Schwen, and Stephen J. Thornton for valuable discussions and acknowledge Anton Paar for use of the MCR 702 rheometer through their VIP academic research program. For this work, I.C., I.G., and M.R. were generously supported by NSF CBET Award Nos.: 2010118, 1804963, and 1509308 and an NSF DMR Award No.: 1507607. B.C. was supported by NSF CBET Award No.: 1916877 and NSF DMR Award No.: 2026834. J.P.S. was supported by NSF Nos. CBET-2010118 and DMR-1719490. E.K. was supported by the NSF Award No.: PHY-1554887, the University of Pennsylvania Materials Research Science and Engineering Center (MRSEC) through Award No.: DMR-1720530. E.D.G. was supported by National Science Foundation (NSF No. DMR-2026842).

AUTHOR DECLARATIONS

Conflict of Interest

The authors have no conflicts to disclose.

DATA AVAILABILITY

The data that support the findings of this study are available from the corresponding author upon reasonable request.

REFERENCES

[1] Brown, E., N. A. Forman, C. S. Orellana, H. Zhang, B. W. Maynor, D. E. Betts, J. M. DeSimone, and H. M. Jaeger, "Generality of shear thickening in dense suspensions," Nat. Mater. **9**, 220–224 (2010).

[2] Wagner, N. J., and J. F. Brady, "Shear thickening in colloidal dispersions," Phys. Today **62**, 27–32 (2009).

[3] Brown, E., and H. M. Jaeger, "Shear thickening in concentrated suspensions: Phenomenology, mechanisms and relations to jamming," Rep. Prog. Phys. **77**, 046602 (2014).

[4] Lin, N. Y., B. M. Guy, M. Hermes, C. Ness, J. Sun, W. C. Poon, and I. Cohen, "Hydrodynamic and contact contributions to continuous shear thickening in colloidal suspensions," Phys. Rev. Lett. **115**, 228304 (2015).

[5] Wyart, M., and M. Cates, "Discontinuous shear thickening without inertia in dense non-Brownian suspensions," Phys. Rev. Lett. **112**, 098302 (2014).

[6] Cates, M. E., and M. Wyart, "Granulation and bistability in non-Brownian suspensions," Rheol. Acta **53**, 755–764 (2014).

[7] Lootens, D., H. Van Damme, Y. Hémar, and P. Hébraud, "Dilatant flow of concentrated suspensions of rough particles," Phys. Rev. Lett. **95**, 268302 (2005).

[8] Seto, R., R. Mari, J. F. Morris, and M. M. Denn, "Discontinuous shear thickening of frictional hard-sphere suspensions," Phys. Rev. Lett. **111**, 218301 (2013).

[9] Brown, E., and H. M. Jaeger, "Dynamic jamming point for shear thickening suspensions," Phys. Rev. Lett. **103**, 086001 (2009).

[10] Hsiao, L. C., S. Jamali, E. Glynos, P. F. Green, R. G. Larson, and M. J. Solomon, "Rheological state diagrams for rough colloids in shear flow," Phys. Rev. Lett. **119**, 158001 (2017).

[11] Hsu, C.-P., S. N. Ramakrishna, M. Zanini, N. D. Spencer, and L. Isa, "Roughness-dependent tribology effects on discontinuous shear thickening," Proc. Natl. Acad. Sci. U.S.A. **115**, 5117–5122 (2018).

[12] Hsu, C.-P., J. Mandal, S. N. Ramakrishna, N. D. Spencer, and L. Isa, "Exploring the roles of roughness, friction and adhesion in discontinuous shear thickening by means of thermo-responsive particles," Nat. Commun. **12**, 1–10 (2021).

[13] Hoffman, R. L., "Explanations for the cause of shear thickening in concentrated colloidal suspensions," J. Rheol. **42**, 111–123 (1998).

[14] Jamali, S., and J. F. Brady, "Alternative frictional model for discontinuous shear thickening of dense suspensions: Hydrodynamics," Phys. Rev. Lett. **123**, 138002 (2019).

[15] More, R., and A. Ardekani, "Roughness induced shear thickening in frictional non-Brownian suspensions: A numerical study," J. Rheol. **64**, 283–297 (2020).

[16] Bourrianne, P., V. Niggel, G. Polly, T. Divoux, and G. H. McKinley, "Tuning the shear thickening of suspensions through surface roughness and physico-chemical interactions," Phys. Rev. Res. **4**, 033062 (2022).

[17] Jaishankar, A., M. Wee, L. Matia-Merino, K. K. Goh, and G. H. McKinley, "Probing hydrogen bond interactions in a shear thickening polysaccharide using nonlinear shear and extensional rheology," Carbohydr. Polym. **123**, 136–145 (2015).

[18] James, N. M., E. Han, R. A. L. de la Cruz, J. Jureller, and H. M. Jaeger, "Interparticle hydrogen bonding can elicit shear jamming in dense suspensions," Nat. Mater. **17**, 965–970 (2018).

[19] James, N. M., C.-P. Hsu, N. D. Spencer, H. M. Jaeger, and L. Isa, "Tuning interparticle hydrogen bonding in shear-jamming suspensions: Kinetic effects and consequences for tribology and rheology," J. Phys. Chem. Lett. **10**, 1663–1668 (2019).

[20] Brown, E., H. Zhang, N. A. Forman, B. W. Maynor, D. E. Betts, J. M. DeSimone, and H. M. Jaeger, "Shear thickening and jamming in densely packed suspensions of different particle shapes," Phys. Rev. E **84**, 031408 (2011).

[21] James, N. M., H. Xue, M. Goyal, and H. M. Jaeger, "Controlling shear jamming in dense suspensions via the particle aspect ratio," Soft Matter **15**, 3649–3654 (2019).

[22] Rathee, V., S. Arora, D. L. Blair, J. S. Urbach, A. Sood, and R. Ganapathy, "Role of particle orientational order during shear thickening in suspensions of colloidal rods," Phys. Rev. E **101**, 040601 (2020).

[23] Guy, B. M., C. Ness, M. Hermes, L. J. Sawiak, J. Sun, and W. C. Poon, "Testing the Wyart–Cates model for non-Brownian shear thickening using bidisperse suspensions," Soft Matter **16**, 229–237 (2020).

[24] Bender, J., and N. J. Wagner, "Reversible shear thickening in monodisperse and bidisperse colloidal dispersions," J. Rheol. **40**, 899–916 (1996).

[25] Ness, C., R. Mari, and M. E. Cates, "Shaken and stirred: Random organization reduces viscosity and dissipation in granular suspensions," Sci. Adv. **4**, eaar3296 (2018).

[26] Niu, R., M. Ramaswamy, C. Ness, A. Shetty, and I. Cohen, "Tunable solidification of cornstarch under impact: How to make someone walking on cornstarch sink," Sci. Adv. **6**, eaay6661 (2020).

[27] Lin, N. Y., C. Ness, M. E. Cates, J. Sun, and I. Cohen, "Tunable shear thickening in suspensions," Proc. Natl. Acad. Sci. U.S.A. **113**, 10774–10778 (2016).

[28] Sehgal, P., M. Ramaswamy, I. Cohen, and B. J. Kirby, "Using acoustic perturbations to dynamically tune shear thickening in colloidal suspensions," Phys. Rev. Lett. **123**, 128001 (2019).

[29] Gillissen, J., C. Ness, J. Peterson, H. Wilson, and M. Cates, "Constitutive model for shear-thickening suspensions: Predictions for steady shear with superposed transverse oscillations," J. Rheol. **64**, 353–365 (2020).

[30] Chen, C., M. van de Naald, A. Singh, N. Dolinski, G. Jackson, H. Jaeger, S. Rowan, and J. de Pablo, "Leveraging the polymer glass transition to access thermally-switchable shear jamming suspensions" ACS Central Science, **9**, no. 4 (2023).

[31] Jackson, G. L., J. M. Dennis, N. D. Dolinski, M. van der Naald, H. Kim, C. Eom, S. J. Rowan, and H. M. Jaeger, "Designing stress-adaptive dense suspensions using dynamic covalent chemistry," Macromolecules **55**, 6453–6461 (2022).

[32] Singh, A., R. Mari, M. M. Denn, and J. F. Morris, "A constitutive model for simple shear of dense frictional suspensions," J. Rheol. **62**, 457–468 (2018).

[33] Royer, J. R., D. L. Blair, and S. D. Hudson, "Rheological signature of frictional interactions in shear thickening suspensions," Phys. Rev. Lett. **116**, 188301 (2016).

[34] Lee, Y.-F., Y. Luo, S. C. Brown, and N. J. Wagner, "Experimental test of a frictional contact model for shear thickening in concentrated colloidal suspensions," J. Rheol. **64**, 267–282 (2020).

[35] Gillissen, J. J., C. Ness, J. D. Peterson, H. J. Wilson, and M. E. Cates, "Constitutive model for time-dependent flows of shear-thickening suspensions," Phys. Rev. Lett. **123**, 214504 (2019).

[36] Pradeep, S., A. R. Jacob, and L. C. Hsiao, "Jamming distance dictates colloidal shear thickening," Phys. Rev. Lett. **127**(15) 158002 (2021).

[37] Liarte, D. B., X. Mao, O. Stenull, and T. Lubensky, "Jamming as a multicritical point," Phys. Rev. Lett. **122**, 128006 (2019).

[38] Goodrich, C. P., S. Dagois-Bohy, B. P. Tighe, M. Van Hecke, A. J. Liu, and S. R. Nagel, "Jamming in finite systems: Stability, anisotropy, fluctuations, and scaling," Phys. Rev. E **90**, 022138 (2014).

[39] Liu, A. J., S. A. Ridout, and J. P. Sethna, "Universal scaling function ansatz for finite-temperature jamming," preprint arXiv:2304.11152 (2023).

[40] Liarte, D. B., S. J. Thornton, E. Schwen, I. Cohen, D. Chowdhury, and J. P. Sethna, "Scaling of dynamical susceptibility at the onset of rigidity for disordered viscoelastic matter," preprint arXiv:2103.07474 (2021).

[41] Liarte, D. B., S. J. Thornton, E. Schwen, I. Cohen, D. Chowdhury, and J. P. Sethna, "Universal scaling for disordered viscoelastic matter near the onset of rigidity," Phys. Rev. E **106**, L052601 (2022).

[42] Cardy, J., *Scaling and Renormalization in Statistical Physics* (Cambridge University, Cambridge, 1996), Vol. 5.

[43] Sachdev, S., *Quantum Phase Transitions* (Cambridge University, Cambridge, 2011).

[44] Sachdev, S., "Theory of finite-temperature crossovers near quantum critical points close to, or above, their upper-critical dimension," Phys. Rev. B **55**, 142–163 (1997).

[45] Sachdev, S., "Universal relaxational dynamics near two-dimensional quantum critical points," Phys. Rev. B **59**, 14054–14073 (1999).

[46] Adam, S., P. W. Brouwer, J. P. Sethna, and X. Waintal, "Enhanced mesoscopic fluctuations in the crossover between random-matrix ensembles," Phys. Rev. B **66**, 165310 (2002).

[47] Chen, Y., S. Zapperi, and J. P. Sethna, "Crossover behavior in interface depinning," Phys. Rev. E **92**, 022146 (2015).

[48] Guy, B., M. Hermes, and W. C. Poon, "Towards a unified description of the rheology of hard-particle suspensions," Phys. Rev. Lett. **115**, 088304 (2015).

[49] We find that the scaling functions for cornstarch silica differ by a multiplicative factor of ∼2, which simply reflects a different solvent viscosity.

[50] Guazzelli, É., and O. Pouliquen, "Rheology of dense granular suspensions," J. Fluid Mech. **852**, P1 (2018).
[51] Morris, J. F., and F. Boulay, "Curvilinear flows of noncolloidal suspensions: The role of normal stresses," J. Rheol. **43**, 1213–1237 (1999).
[52] To construct this phase diagram, we use an extended data set with data closer to x_c. See the supplementary material [78] for more details.
[53] Peters, I. R., S. Majumdar, and H. M. Jaeger, "Direct observation of dynamic shear jamming in dense suspensions," Nature **532**, 214–217 (2016).
[54] Bi, D., J. Zhang, B. Chakraborty, and R. P. Behringer, "Jamming by shear," Nature **480**, 355–358 (2011).
[55] Gameiro, M., A. Singh, L. Kondic, K. Mischaikow, and J. F. Morris, "Interaction network analysis in shear thickening suspensions," Phys. Rev. Fluids **5**, 034307 (2020).
[56] Singh, A., C. Ness, R. Seto, J. J. de Pablo, and H. M. Jaeger, "Shear thickening and jamming of dense suspensions: The 'roll' of friction," Phys. Rev. Lett. **124**, 248005 (2020).
[57] Baumgarten, A. S., and K. Kamrin, "A general constitutive model for dense, fine-particle suspensions validated in many geometries," Proc. Natl. Acad. Sci. U.S.A. **116**, 20828–20836 (2019).
[58] van der Naald, M., A. Singh, T. Eid, K. Tang, J. de Pablo, and H. Jaeger, "Minimally rigid clusters in dense suspension flow" (2023).
[59] van der Naald, M., L. Zhao, G. L. Jackson, and H. M. Jaeger, "The role of solvent molecular weight in shear thickening and shear jamming," Soft Matter **17**, 3144–3152 (2021).
[60] Townsend, A. K., and H. J. Wilson, "Frictional shear thickening in suspensions: The effect of rigid asperities," Phys. Fluids **29**, 121607 (2017).
[61] O'Neill, R. E., J. R. Royer, and W. C. Poon, "Liquid migration in shear thickening suspensions flowing through constrictions," Phys. Rev. Lett. **123**, 128002 (2019).
[62] White, E. E. B., M. Chellamuthu, and J. P. Rothstein, "Extensional rheology of a shear-thickening cornstarch and water suspension," Rheol. Acta **49**, 119–129 (2010).
[63] Han, E., M. Wyart, I. R. Peters, and H. M. Jaeger, "Shear fronts in shear-thickening suspensions," Phys. Rev. Fluids **3**, 073301 (2018).
[64] DeGiuli, E., G. Düring, E. Lerner, and M. Wyart, "Unified theory of inertial granular flows and non-Brownian suspensions," Phys. Rev. E **91**, 062206 (2015).
[65] Boyer, F., É. Guazzelli, and O. Pouliquen, "Unifying suspension and granular rheology," Phys. Rev. Lett. **107**, 188301 (2011).
[66] Perrin, H., C. Clavaud, M. Wyart, B. Metzger, and Y. Forterre, "Interparticle friction leads to nonmonotonic flow curves and hysteresis in viscous suspensions," Phys. Rev. X **9**, 031027 (2019).
[67] Perrin, H., M. Wyart, B. Metzger, and Y. Forterre, "Nonlocal effects reflect the jamming criticality in frictionless granular flows down inclines," Phys. Rev. Lett. **126**, 228002 (2021).
[68] Malbranche, N., A. Santra, B. Chakraborty, and J. F. Morris, "Scaling analysis of shear thickening suspensions," Front. Phys. **10**, 946221 (2022).
[69] Malbranche, N., B. Chakraborty, and J. F. Morris, "Shear thickening in dense bidisperse suspensions," J. Rheol. **67**, 91–104 (2023).
[70] Mari, R., R. Seto, J. F. Morris, and M. M. Denn, "Shear thickening, frictionless and frictional rheologies in non-Brownian suspensions," J. Rheol. **58**, 1693–1724 (2014).
[71] Just as one defines, $u_h(P, T)$ as the magnetic-field like perturbation away from the liquid-gas critical point [42]. Usually, analytic corrections to scaling are treated perturbatively near criticality. Here, we use them to extend our theory to the entire shear-thickening regime.
[72] Goodrich, C. P., A. J. Liu, and J. P. Sethna, "Scaling ansatz for the jamming transition," Proc. Natl. Acad. Sci. U.S.A. **113**, 9745–9750 (2016).
[73] O'hern, C. S., L. E. Silbert, A. J. Liu, and S. R. Nagel, "Jamming at zero temperature and zero applied stress: The epitome of disorder," Phys. Rev. E **68**, 011306 (2003).
[74] Aharony, A., and M. E. Fisher, "Universality in analytic corrections to scaling for planar Ising models," Phys. Rev. Lett. **45**, 679–682 (1980).
[75] Dong, J., and M. Trulsson, "Unifying viscous and inertial regimes of discontinuous shear thickening suspensions," J. Rheol. **64**, 255–266 (2020).
[76] Liu, K., S. Henkes, and J. Schwarz, "Frictional rigidity percolation: A new universality class and its superuniversal connections through minimal rigidity proliferation," Phys. Rev. X **9**, 021006 (2019).
[77] Liu, K., J. E. Kollmer, K. E. Daniels, J. Schwarz, and S. Henkes, "Spongelike rigid structures in frictional granular packings," Phys. Rev. Lett. **126**, 088002 (2021).
[78] See the supplementary material online for details of the sample preparation and experimental protocols, additional corrections to scaling, higher volume fraction data, and details of obtaining the DST line.